Atmospheric Environment 131 (2016) 424–433

Contents lists available at ScienceDirect

Atmospheric Environment

journal homepage: www.elsevier.com/locate/atmosenv

SOA formation from naphthalene, 1-methylnaphthalene, and 2-methylnaphthalene photooxidation

Chia-Li Chen [a, b], Mary Kacarab [a, b], Ping Tang [b], David R. Cocker III [a, b, *]

[a] University of California, Riverside, Department of Chemical and Environmental Engineering, Riverside, CA, USA
[b] College of Engineering – Center for Environmental Research and Technology (CE-CERT), Riverside, USA

HIGHLIGHTS

- High SOA yields from 2-ring PAH photooxidation were found.
- Fractal-like and solid SOA was observed for the methylnaphthalene isomers during high NO_x photooxidation.
- A m/z 104 peak was observed as a marker of phthalic acid from PAH photoxidation by HR-ToF-AMS analysis.

ARTICLE INFO

Article history:
Received 5 October 2015
Received in revised form
22 January 2016
Accepted 4 February 2016
Available online 16 February 2016

Keywords:
SOA yield
m/z 104
Naphthalene
Methylnaphthalene
PAH
Fractal agglomerate

ABSTRACT

The SOA yield and chemical characteristics of SOA formation from naphthalene and two methyl substituted naphthalenes, 1-methylnaphthalene and 2-methylnaphthalene, were studied for high NO_x, low NO_x, and ultra-low NO_x conditions. The SOA yields are high compared to previous studies for all three PAHs precursors: 1-methylnaphthalene > 2-methylnaphthalene ~ naphthalene for all atmospheric conditions studied. The SOA yields range from 0.03 to 0.60 for naphthalene, 0.21–1.52 for 1-methylnaphthalene, and 0.34–0.55 for 2-methylnaphthalene under high NO_x with HONO (initial PAH:NO ratio = 0.03–0.17) conditions. The SOA yield ranges from 0.04 to 0.31 for naphthalene, 0.14–0.72 for 1-methylnaphthalene, and 0.06–0.49 for 2-methylnaphthalene under low NO_x (initial PAH:NO ratio = 0.54–2.20) conditions. SOA yields were substantially greater than 1.0 under H_2O_2 (ultra low NO_x) and low NO_x + H_2O_2 conditions for all three PAH precursors. The system reactivity influenced by OH radicals, NO_x levels, initial PAH/NO ratios, NO_2/NO ratios, and all impacted the SOA formation from the PAH precursors. Fractal-like SOA is observed for the methylnaphthalene isomers during high NO_x photooxidation experiments, implying that researchers studying SOA formation from this precursor must carefully account for particle shape or effective density. A m/z 104 ($C_7H_4O^+$,104.026) peak, consistent with SOA products phthalic acid from earlier studies, was observed as a potential marker of PAH oxidation during HR-ToF-AMS analysis.

1. Introduction

The formation of secondary organic aerosol (SOA) originates from a variety of chemical processes including gas-phase oxidation reactions of organic species, reactions in the particle (condensed) phase and continuing chemistry over multiple generations of oxidation products (Kroll and Seinfeld, 2008). SOA negatively impacts visibility and can affect global radiative forcing through both direct and indirect effects (Kanakidou et al., 2005; Schulz et al., 2006). Additionally, epidemiological evidence shows a significant risk between fine particles and lung cancer, respiratory illness, and cardiovascular disease (Lewtas, 2007).

Polycyclic aromatic hydrocarbons (PAHs) are an important source of semivolatile gas-phase anthropogenic emissions. Sources of PAH include incomplete combustion emissions from vehicles (Shah et al., 2005), biomass burning (Conde et al., 2005; Hedberg et al., 2002), cooking (McDonald et al., 2003), evaporation of petroleum products (Jia and Batterman, 2010), gasoline and diesel fuels (Aislabie et al., 1999). Naphthalene and methylnaphthalenes are the most abundant PAH precursor and may be a major unaccounted for source of secondary organic aerosol (SOA) as their

* Corresponding author. University of California, Riverside, Department of Chemical and Environmental Engineering, Riverside, CA, USA.
E-mail address: dcocker@engr.ucr.edu (D.R. Cocker).

http://dx.doi.org/10.1016/j.atmosenv.2016.02.007
1352-2310/

contribution to ambient secondary particulate matter is not clearly understood The California Air Resources Board (CARB) 2010 California Toxic Inventory (CARB, 2013) estimates the total emissions of naphthalene to be ~910.7 tons year^{-1} in California. Average Southern California Air Basin naphthalene concentrations range from 91 to 445 ng m^{-3} (Eiguren-Fernandez et al., 2004; Lu et al., 2005) with Reisen and Arey reporting much higher naphthalene concentrations in Los Angeles due to heavy traffic emissions than in Riverside (Reisen and Arey, 2005). Pye and Pouliot, 2012 estimated that long-chain alkanes and PAHs accounted for 20–30% of SOA derived from anthropogenic hydrocarbons by Community Multiscale Air Quality (CMAQ) model. Further, Lu et al. simulated the distribution of naphthalene emissions over Southern California using the SMOG airshed model and estimated 10–50 kg day^{-1}grid^{-1} (5-km by 5-km grid cells) in populated urban areas (Lu et al., 2005). However, current SOA model predictions are based on SOA yields from indoor environmental chamber experiments and emission inventory. It is needed to further examine PAH oxidation under different oxidant condition and integrate SOA yields data into current SOA model.

Recent studies have focused on investigating gas-phase chemistry mechanism and particle-phase organic aerosol formation from PAH oxidation. Gas-phase chemistry mechanism and products from OH-initiated reaction of naphthalene and alkylnaphthalene atmospheric oxidation was proposed by Kautzman et al. (2010) and Wang et al. (2007). Kautzman et al. (2010) proposed naphthalene and alkylnaphthalene oxidation mechanisms for high NO_x with 2-formylcinnaldehyde (30–60% yield) as the major product (Nishino et al., 2012; 2009; Sasaki et al., 1997). Formation of nitronaphthalenes (0.6%), naphthols (10%) and other ring-opening and ring-remaining products were observed from OH radical reaction in the presence of NO_x (Sasaki et al., 1997). Additionally, 4-nitro-1-naphthol, hydroxyl phthalic acid and hydroxyl nitrobenzoic acid have also been observed in both urban organic aerosols and laboratory SOA from PAH-NO_x photooxidation (Kautzman et al., 2010). Further, methylnaphthalenes emitted from primary sources can react with OH radicals and NO_x to produce methylnitronaphthalenes and dicarbonyl derivates, which have been reported as carcinogens and associated with mutagenicity and toxic effects in metabolism reactions (Grosovsky et al., 1999; Lin et al., 2009).

SOA yields from PAHs oxidation has been reported by previous studies (Chan et al., 2009; Kautzman et al., 2010; Kleindienst et al., 2012). Chan et al. reported SOA yields for high-NO_x conditions between 0.19 and 0.3 for naphthalene, 0.19 and 0.39 for 1-methylnaphthalene, and 0.26 and 0.45 for 2-methlynaphthalene. Under low-NO_X conditions, SOA yields were observed to be 0.73, 0.68, and 0.58 for naphthalene, 1-methylnaphthalene, 2-methylnaphthalene, respectively (Chan et al., 2009). However, lower PAH SOA yields ranging from 0.02 to 0.22 were observed by Shakya and Griffin (2010) for aerosol mass concentrations less than 10 μg m^{-3} Kleindienst et al. (2012) recently reported that naphthalene SOA yields ranging 0.11–0.27 under higher NO_x conditions, which is much lower than reported by Kautzman et al. (2010). Further, particle-phase phthalic acid has been reported as a major naphthalene photooxidation product for both NO_x conditions, and has been suggested as a potential tracer of ambient naphthalene SOA (Kautzman et al., 2010) due to large observable quantities (e.g., ~14 ng m^{-3} in Birmingham, Al).

The key question in this study is that what the main factors are driving PAH precursor to form SOA. Previous studies from PAH precursor still lack comprehensive understanding characteristics of PAH SOA formation. Overall, this study aims to (i) investigate the roles of NO_x levels and OH radicals on SOA formation from 2 ring-PAH photooxidation; (ii) characterize chemical and physical properties (e.g., volatility, density of particles and chemical composition characteristics) of SOA formation derived from PAHs.

2. Experimental methodology

2.1. Experimental setup

All experiments were performed in the UCR/CE-CERT environmental chamber described in detail elsewhere (Carter et al., 2005). The facility includes a 6 m × 6 m × 12 m thermally insulated enclosure continuously flushed with purified air (Aadco 737 series (Cleves, Ohio) air purification system). Inside the enclosure, there are two 90 m^3 2 mil (54 μm) FEP Teflon® film reactors along with four banks of 115 W 4-ft Sylvania 350BL blacklights, NO_2 photolysis rate (also called k_1) is 0.408 min^{-1}. The blacklight emission spectrum of the irradiation system is particularly between 300 nm and 420 nm with peak wavelength of 350 nm, the region where H_2O_2 has an adequate photolysis rate (Carter et al., 1995). The elevation of the top frames of the reactors are controlled by elevators that slowly move down during the experiments to maintain a positive differential pressure of >0.01 in H_2O thereby reducing likelihood of dilution due to sampling, leaks, and permeation. Prior to inject solid naphthalene (>99%, Sigma Aldrich) and 2-methylnaphthalene (>97%, solid, Sigma-Aldrich) into the oven, naphthalene and 2-methylnaphthalene were prepared by heating up known amount weight and then adhered to glass-wool. Known amount of naphthalene, 1-methylnaphthalene (>95%, liquid, Sigma-Aldrich), 2-methylnaphthalene, and 50% wt hydrogen peroxide (H_2O_2) solution were injected into a glass manifold tube in a 55 °C ~ 60 °C oven, and subsequently flushed into the chamber with purified air for 15 min at 10 L min^{-1} for H_2O_2 and 30 min for PAH, respectively. NO was prepared by filling a calibrated glass bulb with a known pressure of pure NO and then subsequently flushed into the chamber with pure N_2. Nitrous acid (HONO) was injected as the OH precursor for high NO_x (NO > 350 ppb initially) condition experiments. HONO was prepared by adding 10 ml of 1w% $NaNO_2$ dropwise into 20 ml of 10w% H_2SO_4 aqueous solution (Kautzman et al., 2010). A dry air stream was then passed through the bulb, sending HONO into the chamber. When the NO_2 reached about 100 ppb, the injection of HONO was stopped and then the additional NO was added to reach target concentration. H_2O_2 concentration was calculated based on injection volume, %wt of H_2O_2, and chamber volume without accounting for injection and chamber losses. Ammonium sulfate seed aerosol was generated as needed by atomization of a ~0.005 M aqueous ammonium sulfate solution.

2.2. Instrumentation

Gas phase: Perfluorohexane (n-C_6F_{14}) was used as an inert chemical tracer. The perfluorohexane and PAH concentrations were monitored using Agilent 6890 (Palo Alto, CA) gas chromatography (GC) equipped with flame ionization detectors (FID) (equipped with: 30 m × 0.53 mm GS-Alumina column as front detector used for the analysis of light hydrocarbons and perfluorohexane and 30 m × 0.53 mm DB-5 column as back detector used for the analysis of aromatics). The GC column was temperature programmed from −50° (hold 2.0 min) to 40 °C at a rate of 50 °C per minute (hold 1.0 min) then up to 200 °C at a rate of 30 °C per minute with a 13 min hold at the upper limit. A second Agilent 6890 GC equipped with a thermal desorption system (CDS analytical, ACEM9305, Sorbent Tube MX062171 packed with Tenax-TA/Carbopack/Carbosieve S111) was used for the analysis of low-volatility compounds. The tubes were thermally desorbed at 290 °C. The column used was a 30 m Restek® Rtx-35 Amine (0.53 mm ID, 1.00 μm). NO and NO_y-NO were measured by a TECO NO_x analyzer while O_3 was

measured by a Dasibi Environmental Corp. Model 1003-AH O_3 analyzer. It is noted that NO_2 was indirectly measured by the difference of NO_y and NO. The interferences of HONO, nitric acid (HNO_3), organic nitrates ($RONO_2$) and peroxyacetyl nitrates (PANs) in NO_y species measurement were not excluded.

Particle phase: Particle size distributions between 27 and 686 nm and number concentrations were measured with an Scanning Mobility Particle Sizer (SMPS) built in-house described by Cocker et al., 2001. Aerosol particle density was measured with an Aerosol Particle Mass analyzer (APM, Kanomax model 3600) and a SMPS in series. A detailed description of the APM-SMPS system and data algorithms are described elsewhere (Malloy et al., 2009; Nakao et al., 2011). Particle volatility was measured with a volatility tandem differential mobility analyzer (VTDMA) (Nakao et al., 2012; 2011; Qi et al., 2010a, b; Rader and McMurry, 1986), in which monodisperse particles of mobility diameter D_{mi} are selected by the first differential mobility analyzer (DMA) followed by transport through a Dekati thermodenuder (TD, residence time: ~16 s, at 100 °C or at 150 °C). Then, the particle size after the thermodernuder (D_{mf}) is measured by fitting a log-normal size distribution curve acquired by the second DMA. Volume remaining fraction (VRF) is calculated by VRF = $(D_{mf}/D_{mi})^3$ where D_{mf} is the particle mobility diameter after the TD and D_{mi} is the initial particle size selected. The electrostatic FHNW (Fachhochschule Nordwestschweiz) Transmission Electron Microscopy (TEM) sampler was used to collect particles during select experiments. The particulates were subsequently analyzed by TEM (FEI-PHILIPS CM300) at the UCR Central Facility for Advanced Microscopy and Microanalysis (CFAMM).

Particle chemical composition was analyzed with a high-resolution time-of-flight aerosol mass spectrometer (HR-ToF-AMS) operating in "W-mode" (Aiken et al., 2008; 2007; DeCarlo et al., 2006). Details of the HR-ToF-AMS and software analysis are described in DeCarlo et al., 2006. The HR-ToF-AMS data was analyzed by HR-ToF-AMS analysis toolkit 1.51H and PIKA module for SQUIRREL version 1.10H.

3. Results and discussion

3.1. SOA yields from naphthalene, 1-methylnaphthalene and 2-methylnaphthalene

SOA formation from naphthalene, 1-methylnaphthalene and 2-methylnaphthalene was measured for different gas-phase reactivity conditions in the UCR CE-CERT environmental chamber. SOA yields (Y) for individual ROGs were determined as the total aerosol formed divided by mass of PAH consumed. Yield was then plotted versus final organic aerosol mass and fit to the following equation (Odum et al., 1996):

$$Y = M_0 \sum_i \left(\frac{\alpha_i K_{om,i}}{1 + K_{om,i} M_0} \right) \quad (1)$$

To obtain the best fit two product ($i = 2$) model where α_i and $K_{om,i}$ are the mass-based stoichiometric coefficient and absorption equilibrium partitioning coefficient of product *i*, respectively.

An instantaneous aerosol yield (IAY) (Jiang, 2003) was used to compare with reported SOA yield. The IAY can be defined as the aerosol yield at a specific M_0, which is the slope of a tangent line at the point (ΔROG, M_0) on an experimental M_0 versus ΔROG curve (Jiang, 2003). In this study, the IAY for each point is at the irradiation time corresponding to the measured ROG data point.

$$IAY = \frac{d M_0}{d\Delta ROG} \quad (2)$$

All experiments were irradiated (NO_2 photolysis rate(k_1) = 0.408 min^{-1}) under dry conditions (RH< 0.1%). Table 1 lists the experimental conditions and SOA yields for photooxidation experiments conducted for each of the three PAH precursors. The initial PAH concentration in these experiments ranged from 15 ppb to 68 ppb while initial NO_x was >350 ppb for high NO_x experiments and <100 ppb for low NO_x conditions, and ≪1 ppb for H_2O_2 experiments.

3.1.1. High NO_x condition

SOA yield ranged from 0.03 to 0.60 (naphthalene), 0.21–1.52 (1-methylnaphthalene), and 0.34–0.55 (2-methylnaphthalene) under high NO_x (initial PAHs/NO = 0.03–0.17) conditions (Table 1). HONO was injected into high NO_x experiments to serve as an OH radical source to help increase the reactivity of the experiment. However, the HONO production method also produced additional NO and NO_2 which were injected into the chamber. Since NO_2 concentration was not directly measured by a chemiluminescence NO_x analyzer, possible interference from HONO would lead to higher NO_2. The OH radical produced from HONO and NO_2/NO ratio affects aerosol formation from a given PAH precursor (Fig. S1). The lowest SOA yield was observed in the 1732A naphthalene-high NO_x experiment (little HONO injection), an indication of lower OH radicals and NO, and higher NO of 624 ppb, leading to less aerosol formation.

To further investigate the effect of NO_2/NO ratios on PAH SOA formation under high NO_x conditions, the relationship between IAYs and NO_2/NO ratios are shown in Fig. S2. If the initial NO_2/NO ratios ≤0.54, the IAYs increase as NO_2/NO ratios increase. If the initial NO_2/NO ratios ≥0.60, the NO_2/NO ratios vary as the IAYs increase. As the NO_2/NO ratios increase to a threshold, subsequently they decrease as instantaneous yields increase (e.g., 1623A, 1628A, 1590A), indicating the reaction of NO + RO_2 completely forms RO + NO_2 during the course of experiments. In the presence of NO_x, the effect arises from the chain termination in the RO_2 and NO_x cycles via organic nitrates ($RONO_2$) production: RO_2 +NO → $RONO_2$. RO_2 radicals may also react with NO_2 to form peroxynitates ($ROONO_2$): RO_2 +NO_2 →$ROONO_2$. The other possible chain primary termination reaction in PAH oxidation reaction could occur at nitric acid (HNO_3) production in high NO_x region: OH + NO_2 → HNO_3.

The OH radical initiates reactions of alkylnaphthalene/naphthalene mainly by addition to the ring to form an OH-alkylnaphthalene or OH-naphthalene adduct which subsequently reacts with NO_2 or O_2 (Atkinson and Arey, 2007). 1-Methylnaphthalene and 2-methylnaphthalene can also undergo additional reactions with OH, namely H-atom abstraction from the methyl group. In this study, SOA yield under high-NO_x conditions is non-linearly related to the HONO, NO, and NO_2 concentrations (Fig. S1 and Fig. S2), implying that aerosol formation is expected through NO_2 reaction with OH-naphthalene or OH-alkylnaphthalene adducts leading to nitro-containing and other low volatility products. Previous studies have identified ring-opened products from OH-initiated naphthalene or alkylnaphthalene reactions including 2-formylcinnamaldehyde (30–60%), phthaldialdehyde and phthalic anhydride (Atkinson and Arey, 2007; Nishino et al., 2012; 2009). These products can continue to oxidize and form secondary-generation products that could further to partition into the condensed phase.

3.1.2. Low NO_x condition

In the low NO_x (initial PAH/NO = 0.54–2.20) experiments, SOA yield is 0.04–0.31, 0.14–0.72, and 0.06–0.49 for naphthalene, 1-methylnaphthalene, and 2-methylnaphthalene, respectively. The photooxidation routes to form SOA are expected to be dominated by RO_2+HO_2 and RO_2+NO reaction pathways (Kroll and Seinfeld,

Table 1
Initial experimental conditions and SOA yields for all experiments.

High-NO_x (with HONO)		HC_0	ΔHC	NO^a	NO_2^a	NO^b	NO_2^b	ΔM_0	SOA yield[c]	Density
Run ID	Compound	ppb	μg/m^3	ppb	ppb	ppb	ppb	μg/m^3		g/cm^3
1586A	naphthalene	45.3	168	73	94	510	188	94.8	0.60	1.48[d]
1588A	naphthalene	29.1	126	N.D.	104	610	166	59.4	0.47	1.48[d]
1590A	naphthalene	25.9	116	20	142	420	338	47.1	0.41	1.47
1732A	naphthalene	29.6	105	25	38	624	152	3.0	0.03	1.51
1737A	naphthalene	22.6	80	50	88	576	207	20.3	0.25	1.40
1623A	1-methylnaphthalene	67.7	362	44	177	396	440	375.2	1.04	0.92 (1.47 → 0.71)
1628A	1-methylnaphthalene	40.0	203	26	103	397	372	173.7	0.78	1.07 (1.49 → 0.83)
1652A	1-methylnaphthalene	14.2	52	68	50	476	284	10.4	0.21	1.25[e]
1659A	1-methylnaphthalene	26.8	111	63	81	445	341	74.1	0.65	1.25 (1.54 → 1.06)
1770A	1-methylnaphthalene	47.0	253	294	202	400	216	383.2	1.52	1.23 (1.48 → 1.12)
1632A	2-methylnaphthalene	30.6	148	28	77	380	321	51.1	0.35	1.32
1635A	2-methylnaphthalene	41.2	211	47	83	403	348	89.7	0.43	1.26
1768A	2-methylnaphthalene	47.7	182	145	104	530	168	61.1	0.34	1.35
1775A	2-methylnaphthalene	43.7	163	148	117	515	145	89.1	0.55	1.32
Low NO_x condition		HC_0	ΔHC	NO^a	AS[g] seed (μm^3/cm^3)			ΔM_0	Y	Density
1592A	naphthalene	28.0	135	22				5.7	0.04	1.48
1660A	naphthalene + AS	17.1	86	14	17.3			15.5	0.18	1.58
1661A	naphthalene	14.7	76	13				21.1	0.28	1.47
1668A	naphthalene + AS	15.9	77	21	41.9			9.7	0.13	1.61
1718A	naphthalene	27.1	140	19				30.8	0.22	1.48
1828A	naphthalene	34.7	173	10				50.1	0.29	1.48[d]
1992A	naphthalene + AS	27.0	125	18	15.4			34.5	0.28	1.58
1992B	naphthalene	28.7	142	18				27.1	0.19	1.48
2040A	naphthalene + AS	14.6	69	10	3.4			22.7	0.33	1.48
2040B	naphthalene	16.9	84	11				26.2	0.31	1.48 [d]
1616A	1-methylnaphthalene	34.8	114	63				18.7	0.14	1.41
1616B	1-methylnaphthalene	35.0	185	29				34.8	0.19	1.4[f]
1742A	1-methylnaphthalene	45.3	218	71				44.1	0.20	1.44
1664A	1-methylnaphthalene	25.9	148	13				107.0	0.72	1.40
1666A	2-methylnaphthalene	20.0	115	12				56.3	0.49	1.37
1744A	2-methylnaphthalene	26.4	152	49				8.5	0.06	1.40
1745A	2-methylnaphthalene	29.1	157	13				43.4	0.28	1.33
H_2O_2/H_2O_2 + low NO_x conditions				NO^a	H_2O_2 (ppm)			ΔM_0	Y	Density
1584A	naphthalene	24.6	114	–	2			68.5	0.62	1.48[d]
1585A	naphthalene	48.0	313	–	2			201.0	0.96	1.48[d]
1754A	naphthalene	20.8	100	–	1			87.4	0.58	1.48[d]
1776A	naphthalene	46.5	207	–	1			190.3	0.95	1.49
1596A	1-methylnaphthalene	35.6	201	–	1			234.5	1.19	1.4[f]
1598A	1-methylnaphthalene	24.8	139	–	1			164.9	1.19	1.4[f]
1600A	1-methylnaphthalene	50.7	274	–	1			483.2	1.81	1.37
1608A	2-methylnaphthalene	28.6	162	–	1			128.7	0.81	1.39
1772A	2-methylnaphthalene	40.9	232	–	1			202.8	0.87	1.37
1613A	naphthalene	34.8	181	59	1			208.3	1.15	1.43
1650A	1-methylnaphthalene	36.6	209	38	1			403.4	1.93	1.26 (1.49 → 1.05)
1643A	2-methylnaphthalene	34.0	195	55	1			246.5	1.26	1.30

a: initial NO and NO_2 concentration when injecting HONO; b: initial NO and NO_2 concentration after injecting additional NO and mixing reactors before turning blacklights on; c: SOA yield is calculated at the end of each experiment. Each experiment irradiates for 6–8 h d: assume average density of naphthalene SOA is 1.48 g/cm^3.e: assume average density of 1-methylnaphthalene high NO_x SOA is 1.25 g/cm^3; f: assume density of 1-methylnaphthalene H_2O_2+ low NO_x SOA is 1.4 g/cm^3; g: AS: ammonium sulfate.

2008). The SOA yield from the PAH precursors under low-NO_x conditions (NO < 100 ppb and initial PAH/NO ratio = 0.54–2.20) is mostly lower than that observed for high NO_x (NO > 400 ppb and initial PAH/NO ratio = 0.03–0.17) (3.1.1; see also Fig. S1 and Fig. S3) in this study. Fig. S3 shows that the initial PAH/NO ratio significantly influences the SOA growth, which was observed as the initial PAH/NO ratio increases the aerosol formation increases. For instance, the initial naphthalene/NO ratio is 3.41 for 1828A and 1.26 for 1592A, the aerosol mass produced for 1828A is much higher than 1592A as shown in Fig. S3 (a). The SOA yield increased as initial NO level (<100 ppb) decreased which can be attributable to increasing RO_2 and HO_2 radical concentrations leading to reactions forming products with lower volatilities, similar to observed NO_x effects on SOA formation from aromatic hydrocarbon (Li et al., 2015). Organic aerosol does not grow in the early hours of the experiment (e.g., run 1661A) with only slight aerosol formation observed after 3–5 h, suggesting NO_x might slowly react with intermediate radicals forming organic nitrate products.

3.1.3. Effect of seed aerosol

Ammonium sulfate seed aerosol was introduced to four naphthalene low NO_x condition photooxidation experiments with particulate mass of organic aerosol determined by:

$$PM\ mass = PM_{(NH_4)_2SO_4}\ mass + PM_{Org}\ mass + PM_{NO_3}\ mass \quad (3)$$

$$PM_{Org+NO_3}\ mass(t) = (PM\ volume\ corrected \times \rho(t)) \times \left(1 - f_{(NH_4)_2SO_4}(t)\right) \quad (4)$$

where $f_{(NH_4)_2SO_4}$ is the fraction of particulate matter that is ammonium sulfate acquired by HR-ToF-AMS and obtained from eq (3). Aerosol density as a function of time ($\rho(t)$) was directly obtained by the APM-SMPS. Thus, total organic and nitrate aerosol

mass formed (PM_{Org+NO_3} *mass* (*t*)) can be calculated by equation (4). Nitrates also describe the functional group organic nitrates ($RONO_2$). The aerosol formation in the four seeded experiments agrees well with the non-seeded experiments indicating little loss of semi-volatiles to the chamber walls in contrast to Kautzman et al., 2010. This may be due to the large volume of the environmental chamber and the absorption of semi-volatiles to organic matters adsorbed on the inner surface of chamber (Loza et al., 2010). The inner surface of this chamber would be cleaner than that of the chamber used by Kautzman et al., 2010.

3.1.4. H_2O_2/H_2O_2+low NO_x condition

SOA yields in the presence of H_2O_2 increase greatly for naphthalene, 1-methylnaphthalene and 2-methylnaphthalene, with some mass-yields exceeding 1.0. High SOA yields occurred in H_2O_2 (only) irradiation condition (1–2 ppm) due to high OH radical concentrations produced by the blacklights (NO_2 photolysis rate is 0.408 min^{-1}). SOA yield from 1-methylnaphthalene photooxidation is the highest followed by naphthalene and 2-methylnaphthalene. Even higher yields are observed for the low $NO_x + H_2O_2$ conditions due to even higher OH radical concentrations with SOA which are highest for 1-methylnaphthalene (1.93), followed by 2-methylnaphthalene (1.26), and naphthalene (1.15). The yields obtained from the H_2O_2 experiments suggest the RO_2+HO_2 chemistry produces a substantial amount of low-volatility hydroperoxides and acids. NO quickly drops to sub-ppb levels during the first hour of irradiation (e.g., run: 1613A), allowing RO_2 and HO_2 to rapidly build and SOA formation to commence (this is compared with ~5 h for low NO_x experiments when NO depletes and SOA formation accelerates). Additionally, Fig. S1(d) shows a linear relationship between instantaneous aerosol yield (IAY) and M_0 concentration. The PAHs were consumed (>99%) after 3 h irradiation under low $NO_x + H_2O_2$ conditions (Fig. S3 (d)) due to the high OH radical level concentrations. The SOA growth curve (ΔM_0 vs. hydrocarbon reacted ΔHC) indicates that SOA continued to grow after hydrocarbon reacted completely (Fig. S3 (d) 1613A) suggesting partitioning of some multigenerational oxidation products.

3.1.5. Overall comparison

SOA yields are much higher in this work than the studies of Chan et al. (2009), Kleindienst et al. (2012), and Shakya and Griffin (2010) as shown in Table 2. The differences between this study and other studies are attributed to differing chamber conditions such as light intensity, chamber size and wall-effects, NO_x levels, hydroxyl radical concentrations, and organic mass loading. The organic mass loading ranges from 3 to 483 μg m^{-3} in this study, whereas at organic mass loading <50 μg m^{-3}, the SOA yields are comparable to previous studies. Fig. S1 shows that the instantaneous aerosol yield (IAY) trends as: H_2O_2 + low NO_x > H_2O_2 without NO_x > high NO_x (with HONO) > low NO_x conditions. The IAY increases with OH radical increasing as well as with increasing reaction rate with OH (k_{OH}). The system reactivity influenced by H_2O_2, NO_x levels, initial PAH/NO ratios, NO_2/NO ratios, and all impacted the SOA formation from the PAH precursors. Applying the two-product model (eq (1)) to all naphthalene, 1-methylnaphthalene and 2-methylnaphthalene photooxidation experiments (Fig. 1) shows one SOA yield fit curve for the three precursors at higher organic

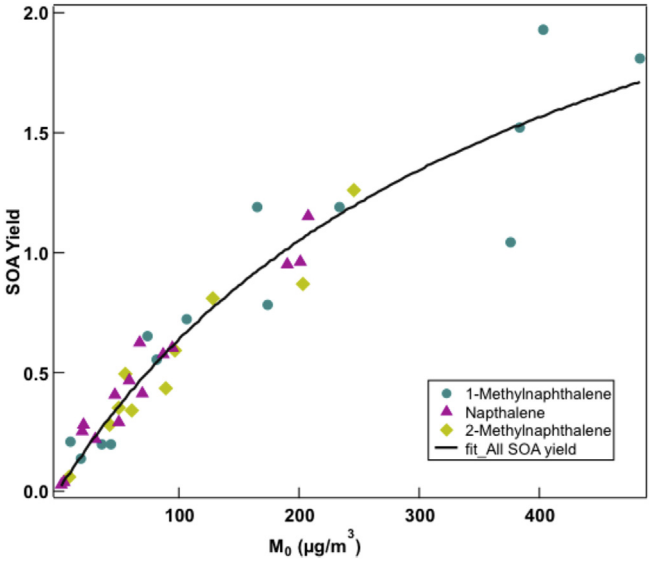

Fig. 1. Two-product model curve for SOA yield from naphthalene, 1-methylnaphthalene and 2-methylnaphthalene photooxidation. Curve is fit with the values 0.9880, 0.0014, 2.2153, and 0.0030 for α_1, $K_{om,1}$, α_2, and $K_{om,2}$, respectively.

Table 2
Comparison of SOA yield from PAHs photooxidation.

PAHs	Condition	SOA yield (Chan et al., 2009)[a]	SOA yield (Kleindienst et al., 2012)[b]	SOA yield (Shakya and Griffin, 2010)[d]	SOA yield (this study)
naphthalene	high NO_x	0.19–0.30	0.28[c]	0.08–0.16	0.03–0.60
naphthalene	low $NO_x + H_2O_2$	0.73	–	–	1.15
naphthalene	low NO_x	–	–	–	0.04–0.33
naphthalene	H_2O_2	–	0.18–0.36	–	0.58–0.96
1-		methylnaphthalene	high NO_x	0.19–0.39	0.20
0.03–0.22	0.21–1.52				
1-		methylnaphthalene	low $NO_x + H_2O_2$	0.68	0.41
–	1.93				
1-		methylnaphthalene	H_2O_2	–	–
–	1.19–1.81				
1-		methylnaphthalene	low NO_x	–	–
–	0.14–0.72				
2-		methylnaphthalene	high NO_x	0.26–0.45	0.15
0.04–0.13	0.34–0.55				
2-		methylnaphthalene	low $NO_x + H_2O_2$	0.58	0.64
–	1.26				
2-		methylnaphthalene	H_2O_2	–	–
–	0.81–0.87				
2-		methylnaphthalene	low NO_x	–	–
–	0.06–0.49				

a: aerosol mass loadings (ΔM_0): 10–40 μg/m^3; b: aerosol mass loadings (ΔM_0): 39–130 μg/m^3; c: 0.14 ppm CH_3ONO, 300 ppb NO for ΔM_0 100 μg/cm^3; d: aerosol mass loadings (ΔM_0): 4–18 μg/m^3.

mass loading range, which indicates the high potential SOA yields among these PAHs. Since the chemical properties such as solid/liquid phase, vapor pressure, and chemical reaction mechanism differ for these three compounds, it was observed that 1-methylnaphthalene presents the highest PAHs precursor that forms the highest SOA yield under similar condition. Overall, the potential PAH SOA precursor yields an order of 1-methylnaphthalene > 2-methylnaphthalene ≈ naphthalene.

3.2. Density of SOA evolution

The SOA density measured by the APM-SMPS is displayed as a function of time (Fig. 2). The initial SOA densities were ~1.58 g cm^{-3} for all experiments, decreasing to ~1.3–1.4 g cm^{-3} and remaining constant during the remainder of the experiment under most conditions, in agreement with a previous aromatic SOA study (Nakao et al., 2013). However, the SOA density decreased continuously for 1-methylnaphthalene photooxidation and 2-merthylnaphthalene under high NO_x conditions (Run ID: 1659A, 1628A, 1623A, 1632A, and 1635A). For these experiments, densities were observed to drop lower than 1 g cm^{-3}, suggesting that the particles are fractal-like (e.g., run 1623A density dropped to 0.7 g cm^{-3}). A power function relationship between effective density and size (equation (5)) is used as (Nakao et al., 2011; Park et al., 2003):

$$\rho_{eff} = C d_m^{D_f - 3} \quad (5)$$

where ρ_{eff} is the effective density of particles, C is a constant, d_m is the mobility diameter of particles, and D_f is the fractal dimension. D_f is 1 for fractal pattern describing straight chain, D_f is 2 for describing surface sheet, and D_f is 3 for describing spherical particle. For example, the fractal dimension (D_f) in experiment 1623A ranges from 3 to 2.31 over the course of experiment (Figure S4(a)). For these experiments, particle number concentrations of ~10^5 particles cm^{-3} are observed (Figure S4(b)) yielding a time constant for coagulation in the order of a few hours (Seinfeld and Pandis, 2006). If the SOA is solid, then it is possible that coagulating particles could form such fractal particles for these conditions and timescales with decreasing particle density. Particle density decreased as their mobility diameter increased from 40 nm to 235 nm (Figure S4(a)). Further evidence of fractal 1-methylnaphthalene SOA was observed by injecting *m*-xylene into the chamber at the end of an experiment. The 1-methylnaphthalene SOA density rapidly increased from 1.15 g cm^{-3} to 1.51 g cm^{-3} as liquid *m*-xylene SOA coated the 1-methylnaphthalene SOA filling the fractal voids (Fig. S5). Finally, a TEM sample was collected during the 1st hour of particle formation, at 5–6 h, and at 6–7 h irradiation time. Fig. 2 shows the TEM images collected of SOA formed from 1-methylnaphthalene under high NO_x photooxidation, confirming the formation of fractal SOA particles coagulated after 5–6 h of photooxidation.

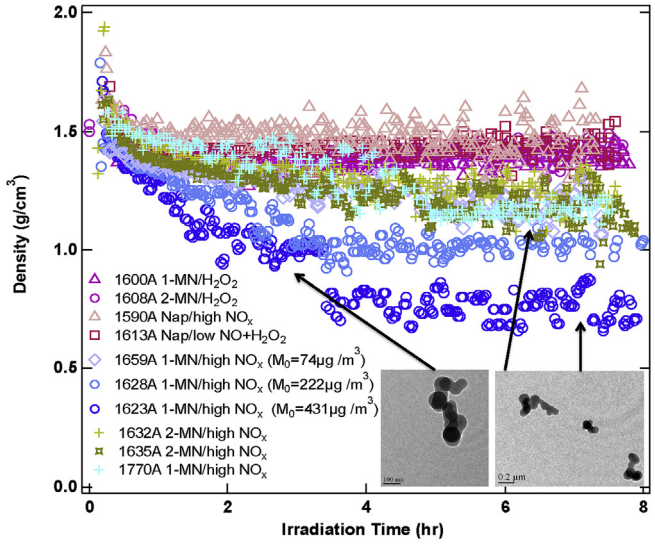

Fig. 2. Time series of the densities of SOA from naphthalene, 1-methylnaphthalene and 2-methlnaphthalene photooxidation under different conditions.

Traditional gas-particle partitioning model usually assume that SOA particles are liquid (Hallquist et al., 2009), but this study presents SOA from 1-methylnaphthalene in environmental chamber can be solid particles with high viscosity under high NO_x condition. This amorphous solid state may influence the partitioning of semi-volatile compounds and inhibit the rate of heterogeneous chemical reactions (Virtanen et al., 2010). Thus, this study challenges traditional views of physical particles phase of SOA formation and demonstrates the importance of measuring density for individual experiments to determine mass based aerosol yield.

3.3. SOA volatility evolution

The volatility trends of strongly decreasing volatility as the experiment progressed were similar for naphthalene, 1-methylnaphthalene and 2-methylnaphthlene photooxidations under high NO_x, H_2O_2 and low NO_x + H_2O_2 conditions. For example, VRF increased from <25% to >85% (Fig. 3(a)) for naphthalene, 1-methylnaphthalene, and 2-methylnaphthalene photooxidation for high-NO_x conditions, even for experiments when the fractal agglomerate formed. This indicates that the vast majority of SOA formed have low volatility even at 100 °C. Additional VTDMA experiments with the thermal denuder temperature set to 150 °C were performed to further explain the volatility of SOA from naphthalene, 1-methylnaphthalene, and 2-methylnaphthalene (Fig. 3(b)), while more SOA evaporated at higher temperature, the SOA at the end of the experiment still has a very low volatility (VRF > 60%). The volatility of the SOA was far lower than that measured for monoaromatic compound, such as VRF increased from 18% to 47% for *m*-xylene photooxidation (Qi et al., 2010a). These results explained that the low volatility of 2-ring PAH photooxidation products undergo condensation, whereas compounds partition from the gas phase 2-ring PAH into the condensed-phase, that produced extremely low volatility oxidation products (e.g., ring-opening acids, nitronaphthalenes, nitromethylnaphthalenes) with different surface and bulk properties that condensed-phase reaction can drive the equilibrium towards particle phase and enhance SOA formation.

3.4. Chemical composition characteristics of SOA formation

The HR-ToF-AMS measures the ion fragments from impaction of particles after vaporization on a heated surface (~600 °C) and electron ionization (70 eV) (DeCarlo et al., 2006). Traces of specific *mass-to-charge* ratios (*m*/*z*) are often used to characterize SOA evolution. Numerous studies have used *m*/*z* 44 (mostly CO_2^+, 43.989) associated with carboxylic acids and *m*/*z* 43 ($C_2H_3O^+$(43.018) or $C_3H_7^+$(43.054)) associated with oxygenated non-acids (such as aldehydes and ketones) as important indicators of chemical composition and aging of chamber SOA and ambient SOA (e.g., Ng et al., 2010; 2011). The *m*/*z* 44 is the key signature of the oxygenated organic compounds formed from PAH SOA formation and the most abundant fragment observed in this study. Typical *m*/*z* distributions of naphthalene, 1-methylnaphthalene and

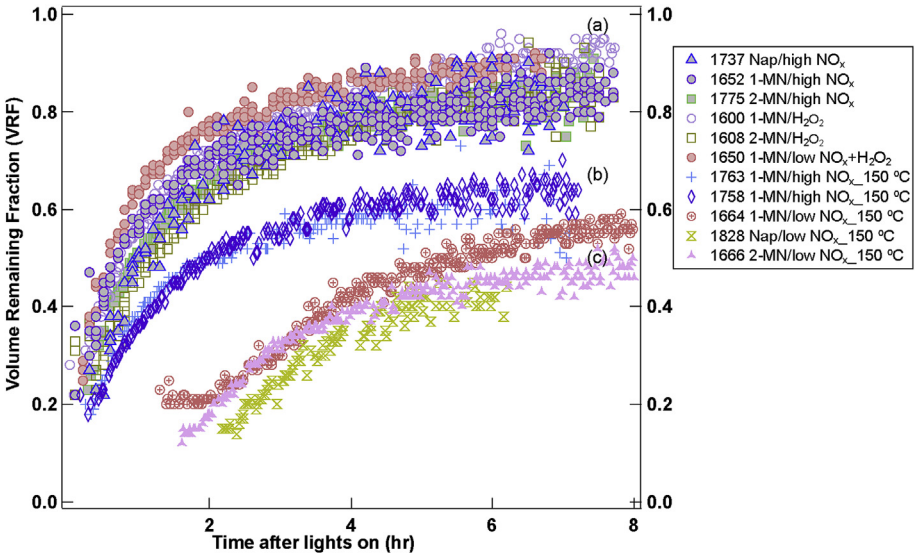

Fig. 3. Volume remaining fraction (VRF) evolution of SOA during the courses of experiments under (a) high NO_x, H_2O_2, low NO_x and H_2O_2 conditions at thermodenuder temperature of 100 °C, (b) high NO_x conditions at 150 °C, (c) low NO_x conditions at 150 °C.

2-methylnaphthalene SOA averaged over the course of the reaction for high-NO_x conditions are shown in Fig. 4. The high m/z 44 signal was paired with a high m/z 18 (H_2O^+) peak implying thermal decomposition of the carboxylic acid group at the vaporizer (Alfarra et al., 2004). Additional major fragment ions detected included m/z 43 ($C_2H_3O^+$, 43.018), m/z 50 ($C_4H_2^+$, 50.156), m/z 51($C_4H_3^+$, 51.023), the typical aromatics series $C_6H_5C_nH_{2n}^+$ (m/z 77 ($C_6H_5^+$, 77.039), 91($C_7H_7^+$, 91.054), 105 ($C_8H_9^+$,105.070)) (McLafferty and Turecek., 1993), m/z 76 ($C_6H_4^+$,76.031), m/z 115 ($C_9H_7^+$,115.054), m/z 104 ($C_8H_8^+$ (104.062) and $C_7H_4O^+$(104.026)), and m/z 105 ($C_7H_5O^+$(105.033) and $C_8H_9^+$(105.070) isomer). Interestingly, nitro-organic compounds fragment ions were also observed at m/z 131 ($C_9H_7O^+$(131.049) and $C_4H_5NO_4^+$(131.021)), m/z 133 ($C_4H_7NO_4^+$ (133.037)) and m/z 145 ($C_{10}H_9O^+$(145.065) and $C_5H_7NO_4^+$(145.037)), corresponding to the N-containing compounds like 2-nitrophenol and 4-nitro-1-naphthol observed during OH-initiated naphthalene/high NO_x photooxidation in Kautzman et al. (2010) study. The chemical structures of these fragments were proposed and summarized in Table S1.

Three possible PAH photooxidation products are proposed in this study based on a m/z comparison to the NIST library WebBook-*trans*-cinnamic acid, phthalic acid, and benzoic acid (Fig. S6). The m/z 147 ($C_9H_7O_2^+$(147.044)) is the expected major ion fragment of *trans*-cinnamic acid ($C_9H_8O_2$, MW 148) with additional fragments of m/z 148, m/z 103, m/z 77, m/z 51, all present in reasonable ratios in the PAH SOA m/z spectrum. C7 (benzoic acid, etc) and C9 compounds (*trans*-cinnamic acid) are secondary products formed through the O_2 addition to 2-formylcinnamaldyhyde to form RO_2 radical that subsequently reacts with NO to form RO radical. It was proposed that loss of CO_2 followed by a hydride shift and oxidation by O_2 and HO_2 would be a possible mechanism to form an acid (Kautzman et al., 2010; Fig. S7, Scheme 1and 2). Additionally, phthalic acid ($C_8H_6O_4$, M.W. 166) is suggested by the major mass spectrum peak at m/z 104 ($C_7H_4O^+$) along with additional at m/z 76, m/z 18, m/z 50, and m/z 148 (Figs. S6 and S8). The m/z 104 mass spectra intensity from each high-NO_x PAH experiment shows that the fraction 104 (f_{104}) is 1.82%, 1.14% and 1.28% for naphthalene, 1-methylnaphthalene, and 2-methylnaphthalene, respectively (Fig. S9). The mechanisms from the OH oxidation of phthaldialdehyde and further oxidized to form phthalic anhydride and phthalic acid were previously proposed (Fig. S7, Scheme 2). Phthalic acid has been identified as major PAH SOA product in previous OH radical-initiated naphthalene reactions (Kautzman et al., 2010; Wang et al., 2007). It is therefore suggested that the m/z 104 can be used as a potential indicator of phthalic acid in HR-ToF-AMS mass spectra distribution from PAH photooxidation. However, because phthalic acid, phthalic anhydride, or phthalic ester can be formed from variety of sources, the m/z 104 use as a marker remains questionable in the ambient measurement.

The triangle plot (f_{44} vs. f_{43}) of SOA formation from naphthalene, 1-methylnaphthalene and 2-methylanpthalene photooxidation for different conditions is shown in Fig. S10. The naphthalene SOA lies on the top section of the triangle area, 1-methylnaphthalene SOA sits on the left edge and 2-methylnaphthalene SOA locates on the right edge of the triangle which is known as ambient OOA (Ng et al., 2010). It is suggested that PAHs SOA is highly oxidized since f_{43} < 0.05 and the H:C is ~1. Interestingly, f_{43} of 2-methylnaphthalene SOA was much higher than 1-methylnaphthalene and naphthalene, suggesting more aldehydes or ketones (CH_2CHO^+ or CH_3CO^+) as well as saturated hydrocarbons ($C_3H_7^+$) (Alfarra et al., 2004) products are formed from 2-methylnaphthalene than the other PAHs. It suggests that the methyl group on 2-ring PAH impacts OH-initiated oxidation of forming first-generation C11 dicarbonyl fragment products (Fig. S11, Scheme 3). As determined by Wang et al. (2007), 48% of the OH addition occurs at the C_2 position for 1-methylnaphthalene, and 53% of the OH addition occurs at C_1 position for 2-methylnaphthalene, both following the breakage of the C_1 and C_2 bond. Further oxidation of first-generation dicarbonyl fragment product from oxidation of 2-methylnaphthalene was proposed as Fig. S11, Scheme 4, suggesting more aldehyde group compounds formed with high m/z 43 fragment.

Under high NO_x conditions, the SOA f_{44} continuously increased from 0.17 to 0.32 during naphthalene photooxidation, which is a much larger increase than observed for 1-methylnaphthalene and 2-methylnaphthalene. The same f_{44} aging trend occurs for the three PAHs precursors under high NO_x, H_2O_2, and low NO_x + H_2O_2 conditions experiments, indicating that the formation of highly oxidized SOA. Chhabra et al. (2010) also reported that higher organic acid concentrations under low-NO_x conditions (H_2O_2 only) from naphthalene oxidation also consistent with the AMS data that characterizes higher f_{44} values and O/C ratios than those of high-

(a) 1629A Naphthalene/high-NO_x

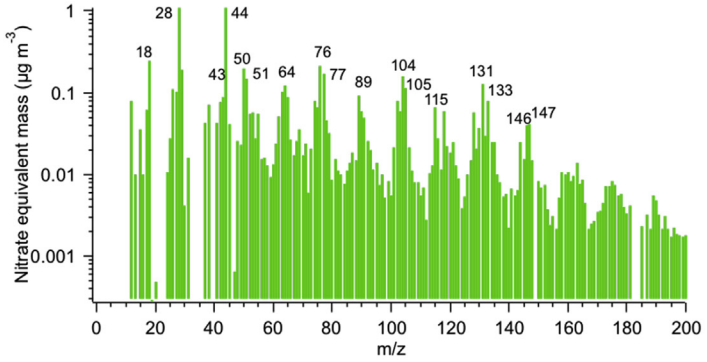

m/z >100	HR-AMS suggested formula		
104	C_7H_4O	C_8H_8	
105	C_7H_5O	C_8H_9	
115	C_9H_7		
131	C_9H_7O	$C_6H_{11}O_3$	$C_4H_5NO_4$
133	$C_4H_7NO_4$	$C_8H_5O_2$	$C_9H_{11}N$
145	$C_5H_7NO_4$	$C_{10}H_9O$	

(b) 1628A 1-Methylnaphthalene/high-NO_x

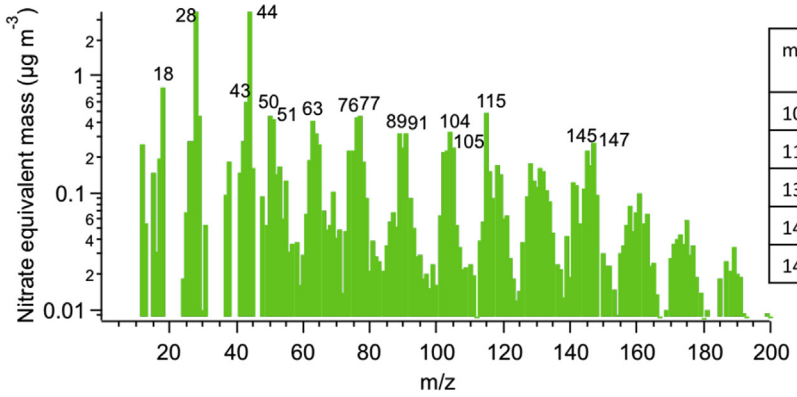

m/z >100	HR-AMS suggested formula	
104	C_8H_8	C_7H_4O
115	C_9H_7	$C_5H_7O_3$
133	$C_4H_7NO_4$	
145	$C_{10}H_9O$	$C_5H_7NO_4$
147	$C_9H_7O_2$	$C_{10}H_{11}O$

(c) 1768A 2-Methylnaphthalene/high-NO_x

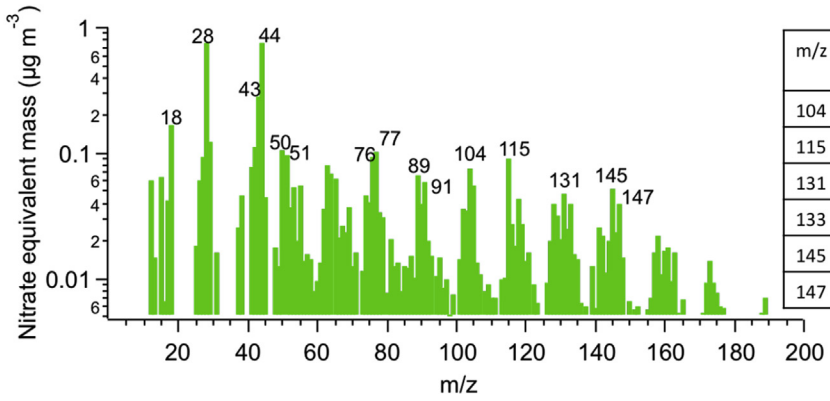

m/z >100	HR-AMS suggested formula	
104	C_7H_4O	C_8H_8
115	C_9H_7	
131	C_9H_7O	$C_4H_5NO_4$
133	$C_4H_7NO_4$	
145	$C_{10}H_9O$	$C_5H_7NO_4$
147	$C_9H_7O_2$	

Fig. 4. HR-ToF-AMS mass spectra distribution of three representative high-NO_x SOA experiments. (a) naphthalene high-NO_x; (b) 1-methylnaphthalene high-NO_x; (c) 2-methylnaphthalene high-NO_x. (see also Figs. S13–S15).

NO_x data, likely due to higher OH exposures.

SOA characteristics including oxygen-to-carbon ratio (O/C), hydrogen-to-carbon ratio (H/C), and VRF are summarized in Table S2. The average O/C ratios of naphthalene and methylnaphthalene SOA increased from 0.33 to 0.63 during the course of the experiment. The H/C ratios for PAH SOA is around 0.9–1.0, which is consistent with Chhabra et al. (2010) study. The average mean oxidation state of carbon ($\overline{OS}_c$), calculated as $\overline{OS}_c \approx 2\,O/C - H/C$ (Kroll et al., 2011), increases from −0.5 to 0.5 over the course of experiment. Fig. S12 shows the Van Krevelen diagram from PAHs photooxidation for each of the PAH precursors. The increasing $\overline{OS}_c$ is consistent with SOA aging during the course of experiment. The naphthalene and methylnaphthalenes SOA was suggested to be between low volatility oxygenated OA (LV-OOA) and SV-OOA compared to ambient OOA in the triangle plot and Van Krevelen diagram as Ng et al. The O/C ratios increased with irradiation time is consistent with f_{44} formation, which further demonstrated that oxidized organic aerosol aging property during PAHs

photooxidation under both NO_x conditions and absence of NO_x conditions. It also confirms that the aromaticity of 2-ring PAH allows for multiple oxidation steps through ring opening and bicyclic peroxy radical routes to form more carboxylic acids and hydroperoxides.

4. Conclusions

The characteristics of naphthalene, 1-methylnaphthalene and 2-methylnaphthalene SOA under high NO_x, low NO_x and the absence of NO_x conditions are reported. SOA yields from naphthalene and methylnaphthalene are high with increasing yields of 1-methylnaphthalene > naphthalene~ 2-methylnaphthalene, differing from the results of earlier studies due to the differences in chamber experimental conditions. The system reactivity influenced by OH radicals, NO_x levels, initial PAH/NO ratios, NO_2/NO ratios, and all impacted the SOA formation from the PAH precursors. It is noted that 1-methylnaphthalene is the highest PAHs precursor that leads to higher SOA potential formation. The CARB emission inventory for toxic shows that naphthalene is the most abundant precursor (910.7 tons/year) among PAHs followed by 2-methylnaphthalene accounting for 81.1 tons/year. Given their high SOA yields, near 1.0, these PAHs can significantly contribute to the aerosol inventory through secondary atmospheric reactions.

Further, it was determined that the phase state of 1-methylnaphthalene and 2-methylnaphthalene/high NO_x SOA is solid allowing it to form fractal-like SOA when particle number is high enough to promote coagulation. Formation of fractal SOA particles requires careful evaluation of SOA density to accurately represent SOA mass yields. The m/z 104 is identified as a possible indicator of phthalic acid from naphthalene photooxidation by HR-ToF-AMS measurement. Finally, the triangle plot, Van Krevelen diagram, and $\overline{OS}_c$ show significant evolution of the SOA during the course of the experiment.

Acknowledgements

This study has been funded by the National Science Foundation (ATM-0449778 and ATM-0901282), and the W. M. Keck Foundation. We would like to acknowledge Kurt Bumiller for experimental setup, and Shunsuke Nakao for helpful discussion, Mary Kacarab for preliminary experiments. Especially, we would like to acknowledge Yue Lin for performing TEM images at UCR Central Facility for Advanced Microscopy and Microanalysis (CFAMM).

Appendix A. Supplementary data

Supplementary data related to this article can be found at http://dx.doi.org/10.1016/j.atmosenv.2016.02.007.

References

Aiken, A.C., DeCarlo, P.F., Jimenez, J.L., 2007. Elemental analysis of organic species with electron ionization high-resolution mass spectrometry. Anal. Chem. 79, 8350–8358. http://dx.doi.org/10.1021/ac071150w.

Aiken, A.C., Decarlo, P.F., Kroll, J.H., Worsnop, D.R., Huffman, J.A., Docherty, K.S., Ulbrich, I.M., Mohr, C., Kimmel, J.R., Sueper, D., Sun, Y., Zhang, Q., Trimborn, A., Northway, M., Ziemann, P.J., Canagaratna, M.R., Onasch, T.B., Alfarra, M.R., Prevot, A.S.H., Dommen, J., Duplissy, J., Metzger, A., Baltensperger, U., Jimenez, J.L., 2008. O/C and OM/OC ratios of primary, secondary, and ambient organic aerosols with high-resolution time-of-flight aerosol mass spectrometry. Environ. Sci. Technol. 42, 4478–4485. http://dx.doi.org/10.1021/es703009q.

Aislabie, J., Balks, M., Astori, N., Stevenson, G., Symons, R., 1999. Polycyclic aromatic hydrocarbons in fuel-oil contaminated soils. Antarct. Chemosphere 39, 2201–2207.

Alfarra, M., Coe, H., Allan, J., Bower, K., Boudries, H., Canagaratna, M., Jimenez, J., Jayne, J., Garforth, A., Li, S., 2004. Characterization of urban and rural organic particulate in the lower Fraser Valley using two aerodyne aerosol mass Spectrometers. Atmos. Environ. 38, 5745–5758. http://dx.doi.org/10.1016/j.atmosenv.2004.01.054.

Atkinson, R., Arey, J., 2007. Mechanisms of the Gas-Phase reactions of aromatic hydrocarbons and PAHS with OH and NO3 radicals. Polycycl. Aromat. Compd. 27, 15–40. http://dx.doi.org/10.1080/10406630601134243.

CARB, 2013. California Toxics Inventory "Draft 2010 CTI Summary Table". Calif. Air Resour. Board.. URL. http://www.arb.ca.gov/toxics/cti/cti.htm

Carter, W.P.L., Cocker III, D.R., Fitz, D.R., Malkina, I.L., Bumiller, K., Sauer, C.G., Pisano, J.T., Bufalino, C., Song, C., 2005. A new environmental chamber for evaluation of gas-phase chemical mechanisms and secondary aerosol formation. Atmos. Environ. 39, 7768–7788. http://dx.doi.org/10.1016/j.atmosenv.2005.08.040.

Carter, W.P.L., Luo, D., Malkina, I.L., Pierce, J.A., 1995. Environmental chamber studies of atmospheric reactivities of volatile organic compounds. Effects of varying chamber and light source; Final report to National Renewable Energy Laboratory;. https://www.cert.ucr.edu/~carter/pubs/explrept.pdf.

Chan, A.W.H., Kautzman, K.E., Chhabra, P.S., Surratt, J.D., Chan, M.N., Crounse, J.D., Kürten, A., Wennberg, P.O., Flagan, R.C., Seinfeld, J.H., 2009. Secondary organic aerosol formation from photooxidation of naphthalene and alkylnaphthalenes: implications for oxidation of intermediate volatility organic compounds (IVOCs). Atmos. Chem. Phys. 9, 3049–3060. http://dx.doi.org/10.5194/acp-9-3049-2009.

Chhabra, P.S., Flagan, R.C., Seinfeld, J.H., 2010. Elemental analysis of chamber organic aerosol using an aerodyne high-resolution aerosol mass spectrometer. Atmos. Chem. Phys 10, 4111–4131. http://dx.doi.org/10.5194/acp-10-4111-2010.

Cocker, D.R., Flagan, R.C., Seinfeld, J.H., 2001. State-of-the-art chamber facility for studying atmospheric aerosol chemistry. Environ. Sci. Technol. 35, 2594–2601. http://dx.doi.org/10.1021/es0019169.

Conde, F.J., Ayala, J.H., Afonso, A.M., González, V., 2005. Emissions of polycyclic aromatic hydrocarbons from combustion of agricultural and sylvicultural debris. Atmos. Environ. 39, 6654–6663. http://dx.doi.org/10.1016/j.atmosenv.2005.07.043.

DeCarlo, P.F., Kimmel, J.R., Trimborn, A., Northway, M.J., Jayne, J.T., Aiken, A.C., Gonin, M., Fuhrer, K., Horvath, T., Docherty, K.S., Worsnop, D.R., Jimenez, J.L., 2006. Field-deployable, high-resolution, time-of-flight aerosol mass spectrometer. Anal. Chem. 78, 8281–8289. http://dx.doi.org/10.1021/ac061249n.

Eiguren-Fernandez, A., Miguel, A.H., Froines, J.R., Thurairatnam, S., Avol, E.L., 2004. Seasonal and spatial variation of polycyclic aromatic hydrocarbons in vapor-phase and PM 2.5 in southern California urban and rural communities. Aerosol Sci. Technol. 38, 447–455. http://dx.doi.org/10.1080/02786820490449511.

Grosovsky, A.J., Sasaki, J.C., Arey, J., Eastmond, D.A., Parks, K.K., Atkinson, R., 1999. Evaluation of the potential health effects of the atmospheric reaction products of polycyclic aromatic hydrocarbons. Res. Rep. Health. Eff. Inst. i–iv, 1–22 discussion 23–27.

Hallquist, M., Wenger, J., Baltensperger, U., Rudich, Y., Simpson, D., Claeys, M., Dommen, J., Donahue, N., George, C., Goldstein, A., et al., 2009. The formation, properties and impact of secondary organic aerosol: current and emerging issues. Atmos. Chem. Phys. 9, 5155–5236.

Hedberg, E., Kristensson, A., Ohlsson, M., Johansson, C., Johansson, P.Å, Swietlicki, E., Vesely, V., Wideqvist, U., Westerholm, R., 2002. Chemical and physical characterization of emissions from birch wood combustion in a wood stove. Atmos. Environ. 36, 4823–4837. http://dx.doi.org/10.1016/S1352-2310(02)00417-X.

Jia, C., Batterman, S., 2010. A critical review of naphthalene sources and exposures relevant to indoor and outdoor air. Int. J. Environ. Res. Public Health 7, 2903–2939. http://dx.doi.org/10.3390/ijerph7072903.

Jiang, W., 2003. Instantaneous secondary organic aerosol yields and their comparison with overall aerosol yields for aromatic and biogenic hydrocarbons. Atmos. Environ. 37, 5439–5444. http://dx.doi.org/10.1016/j.atmosenv.2003.09.018.

Kanakidou, M., Seinfeld, J.H., Pandis, S.N., Barnes, I., Dentener, F.J., Facchini, M.C., Van Dingenen, R., Ervens, B., Nenes, A., Nielsen, C.J., Swietlicki, E., Putaud, J.P., Balkanski, Y., Fuzzi, S., Horth, J., Moortgat, G.K., Winterhalter, R., Myhre, C.E.L., Tsigaridis, K., Vignati, E., Stephanou, E.G., Wilson, J., 2005. Organic aerosol and global climate modelling: a review. Atmos. Chem. Phys. 5, 1053–1123. http://dx.doi.org/10.5194/acp-5-1053-2005.

Kautzman, K.E., Surratt, J.D., Chan, M.N., Chan, A.W.H., Hersey, S.P., Chhabra, P.S., Dalleska, N.F., Wennberg, P.O., Flagan, R.C., Seinfeld, J.H., 2010. Chemical composition of gas- and aerosol-phase products from the photooxidation of naphthalene. J. Phys. Chem. A 114, 913–934. http://dx.doi.org/10.1021/jp908530s.

Kleindienst, T.E., Jaoui, M., Lewandowski, M., Offenberg, J.H., Docherty, K.S., 2012. The formation of SOA and chemical tracer compounds from the photooxidation of naphthalene and its methyl analogs in the presence and absence of nitrogen oxides. Atmos. Chem. Phys. Discuss. 12, 12163–12201. http://dx.doi.org/10.5194/acpd-12-12163-2012.

Kroll, J., Donahue, N., Jimenez, J., 2011. Carbon oxidation state as a metric for describing the chemistry of atmospheric organic aerosol. Nat. Chem. 3, 133–139. http://dx.doi.org/10.1038/nchem.948.

Kroll, J.H., Seinfeld, J.H., 2008. Chemistry of secondary organic aerosol: formation and evolution of low-volatility organics in the atmosphere. Atmos. Environ. 42, 3593–3624. http://dx.doi.org/10.1016/j.atmosenv.2008.01.003.

Lewtas, J., 2007. Air pollution combustion emissions: characterization of causative agents and mechanisms associated with cancer, reproductive, and cardiovascular effects. Mutat. Res. 636, 95–133. http://dx.doi.org/10.1016/j.mrrev.2007.08.003.

Li, L., Tang, P., Cocker, D.R., 2015. Instantaneous nitric oxide effect on secondary

organic aerosol formation from m-xylene photooxidation. Atmos. Environ 119, 144–155. http://dx.doi.org/10.1016/j.atmosenv.2015.08.010.
Lin, C.Y., Wheelock, A.M., Morin, D., Baldwin, R.M., Lee, M.G., Taff, A., Plopper, C., Buckpitt, A., Rohde, A., 2009. Toxicity and metabolism of methylnaphthalenes: comparison with naphthalene and 1-nitronaphthalene. Toxicology 260, 16–27. http://dx.doi.org/10.1016/j.tox.2009.03.002.
Loza, C.L., Chan, A.W.H., Galloway, M.M., Keutsch, F.N., Flagan, R.C., Seinfeld, J.H., 2010. Characterization of vapor wall loss in laboratory chambers. Environ. Sci. Technol. 44, 5074–5078. http://dx.doi.org/10.1021/es100727v.
Lu, R., Wu, J., Turco, R.P., Winer, A.M., Atkinson, R., Arey, J., Paulson, S.E., Lurmann, F.W., Miguel, A.H., Eiguren-Fernandez, A., 2005. Naphthalene distributions and human exposure in southern California. Atmos. Environ. 39, 489–507. http://dx.doi.org/10.1016/j.atmosenv.2004.09.045.
Malloy, Q.G.J., Nakao, S., Qi, L., Austin, R., Stothers, C., Hagino, H., Cocker, D.R., 2009. Real-time aerosol density determination utilizing a modified scanning mobility particle Sizer—Aerosol particle mass analyzer system. Aerosol Sci. Technol. 43, 673–678. http://dx.doi.org/10.1080/02786820902832960.
McDonald, J.D., Zielinska, B., Fujita, E.M., Sagebiel, J.C., Chow, J.C., Watson, J.G., 2003. Emissions from charbroiling and grilling of chicken and beef. J. Air Waste Manag. Assoc. 53, 185–194. http://dx.doi.org/10.1080/10473289.2003.10466141.
McLafferty, F.W., Turecek, F., 1993. Interpretation of Mass Spectra. University Science Books, Sausalito, California. http://dx.doi.org/10.1002/bms.1200230614.
Nakao, S., Liu, Y., Tang, P., Chen, C.-L., Zhang, J., Cocker III, D.R., 2012. Chamber studies of SOA formation from aromatic hydrocarbons: observation of limited glyoxal uptake. Atmos. Chem. Phys. 12, 3927–3937. http://dx.doi.org/10.5194/acp-12-3927-2012.
Nakao, S., Shrivastava, M., Nguyen, A., Jung, H., Cocker, D., 2011. Interpretation of secondary organic aerosol formation from diesel exhaust photooxidation in an environmental chamber. Aerosol Sci. Technol. 45, 964–972. http://dx.doi.org/10.1080/02786826.2011.573510.
Nakao, S., Tang, P., Tang, X., Clark, C.H., Qi, L., Seo, E., Asa-Awuku, A., Cocker, D., 2013. Density and elemental ratios of secondary organic aerosol: application of a density prediction method. Atmos. Environ. 68, 273–277. http://dx.doi.org/10.1016/j.atmosenv.2012.11.006.
Ng, N.L., Canagaratna, M.R., Jimenez, J.L., Chhabra, P.S., Seinfeld, J.H., Worsnop, D.R., 2011. Changes in organic aerosol composition with aging inferred from aerosol mass spectra. Atmos. Chem. Phys. 11, 6465–6474. http://dx.doi.org/10.5194/acp-11-6465-2011.
Ng, N.L., Canagaratna, M.R., Zhang, Q., Jimenez, J.L., Tian, J., Ulbrich, I.M., Kroll, J.H., Docherty, K.S., Chhabra, P.S., Bahreini, R., Murphy, S.M., Seinfeld, J.H., Hildebrandt, L., Donahue, N.M., DeCarlo, P.F., Lanz, V.A., Prévôt, A.S.H., Dinar, E., Rudich, Y., Worsnop, D.R., 2010. Organic aerosol components observed in northern hemispheric datasets from aerosol mass spectrometry. Atmos. Chem. Phys. 10, 4625–4641. http://dx.doi.org/10.5194/acp-10-4625-2010.
Nishino, N., Arey, J., Atkinson, R., 2012. 2-Formylcinnamaldehyde formation yield from the OH radical-initiated reaction of naphthalene: effect of NO(2) concentration. Environ. Sci. Technol. 46, 8198–8204. http://dx.doi.org/10.1021/es301865t.
Nishino, N., Arey, J., Atkinson, R., 2009. Yields of glyoxal and ring-cleavage coproducts from the OH radical-initiated reactions of naphthalene and selected alkylnaphthalenes. Environ. Sci. Technol. 43, 8554–8560. http://dx.doi.org/10.1021/es902018v.
Odum, J.R., Hoffmann, T., Bowman, F., Collins, D., Flagan, R.C., Seinfeld, J.H., 1996. Gas/particle partitioning and secondary organic aerosol yields. Environ. Sci. Technol 30, 2580–2585. http://dx.doi.org/10.1021/es950943+.
Park, K., Cao, F., Kittelson, D.B., McMurry, P.H., 2003. Relationship between particle mass and mobility for diesel exhaust particles. Environ. Sci. Technol. 37, 577–583.
Pye, H.O.T., Pouliot, G.A., 2012. Modeling the role of alkanes, polycyclic aromatic hydrocarbons, and their oligomers in secondary organic aerosol formation. Environ. Sci. Technol. 46, 6041–6047. http://dx.doi.org/10.1021/es300409w.
Qi, L., Nakao, S., Malloy, Q., Warren, B., Cocker III, D.R., 2010a. Can secondary organic aerosol formed in an atmospheric simulation chamber continuously age? Atmos. Environ. 44, 2990–2996. http://dx.doi.org/10.1016/j.atmosenv.2010.05.020.
Qi, L., Nakao, S., Tang, P., Cocker III, D.R., 2010b. Temperature effect on physical and chemical properties of secondary organic aerosol from *m*-xylene photooxidation. Atmos. Chem. Phys. Discuss. 10, 863–883. http://dx.doi.org/10.5194/acpd-10-863-2010.
Rader, D.J., McMurry, P.H., 1986. Application of the tandem differential mobility analyzer to studies of droplet growth or evaporation. J. Aerosol Sci. http://dx.doi.org/10.1016/0021-8502(86)90031-5.
Reisen, F., Arey, J., 2005. Atmospheric reactions influence seasonal PAH and Nitro-PAH concentrations in the Los Angeles Basin. Environ. Sci. Technol. 39, 64–73. http://dx.doi.org/10.1021/es035454l.
Sasaki, J., Aschmann, S.M., Kwok, E.S.C., Atkinson, R., Arey, J., 1997. Products of the Gas-Phase OH and NO 3 radical-initiated reactions of naphthalene. Environ. Sci. Technol. 31, 3173–3179. http://dx.doi.org/10.1021/es9701523.
Schulz, M., Textor, C., Kinne, S., Balkanski, Y., Bauer, S., Berntsen, T., Berglen, T., Boucher, O., Dentener, F., Guibert, S., Isaksen, I.S.A., Iversen, T., Koch, D., Kirkevåg, A., Liu, X., Montanaro, V., Myhre, G., Penner, J.E., Pitari, G., Reddy, S., Seland, Ø., Stier, P., Takemura, T., 2006. Radiative forcing by aerosols as derived from the AeroCom present-day and pre-industrial simulations. Atmos. Chem. Phys. 6, 5225–5246. http://dx.doi.org/10.5194/acp-6-5225-2006.
Seinfeld, J.H., Pandis, S.N., 2006. Atmospheric Chemistry and Physics: from Air Pollution to Climate Change, second ed. John Wiley & Sons, Somerset, NJ, USA.
Shah, S.D., Ogunyoku, T.A., Miller, J.W., Cocker, D.R., 2005. On-road emission rates of PAH and n-alkane compounds from heavy-duty diesel vehicles. Environ. Sci. Technol. 39, 5276–5284. http://dx.doi.org/10.1021/es048086+.
Shakya, K.M., Griffin, R.J., 2010. Secondary organic aerosol from photooxidation of polycyclic aromatic hydrocarbons. Environ. Sci. Technol. 44, 8134–8139. http://dx.doi.org/10.1021/es1019417.
Virtanen, A., Joutsensaari, J., Koop, T., Kannosto, J., Yli-Pirilä, P., Leskinen, J., Mäkelä, J.M., Holopainen, J.K., Pöschl, U., Kulmala, M., Worsnop, D.R., Laaksonen, A., 2010. An amorphous solid state of biogenic secondary organic aerosol particles. Nature 467, 824–827. http://dx.doi.org/10.1038/nature09455.
Wang, L., Atkinson, R., Arey, J., 2007. Dicarbonyl products of the OH radical-initiated reactions of naphthalene and the C1- and C2-alkylnaphthalenes. Environ. Sci. Technol. 41, 2803–2810. http://dx.doi.org/10.1021/es0628102.